ISSN 1063-7834, Physics of the Solid State, 2021, Vol. 63, No. 12, pp. 1795–1810. © Pleiades Publishing, Ltd., 2021.
ISSN 1063-7834, Physics of the Solid State, 2021. © Pleiades Publishing, Ltd., 2021.
Russian Text © The Author(s), 2021, published in Fizika Tverdogo Tela, 2021, Vol. 63, No. 10, pp. 1617–1632.

The Peculiarities of the Spectral Characteristics of Different $Lu_{1-x}RE_xBO_3$ Structural Modifications

S. Z. Shmurak[a, *], V. V. Kedrov[a], A. P. Kiselev[a], T. N. Fursova[a], I. I. Zver'kova[a], and E. Yu. Postnova[a]

[a] *Osipyan Institute of Solid State Physics RAS, Chernogolovka, Moscow oblast, 142432 Russia*

**e-mail: shmurak@issp.ac.ru*

Received April 30, 2021; revised April 30, 2021; accepted May 7, 2021

Abstract—The structure, the IR absorption spectra, and the luminescence spectra of microcrystals of orthoborates $Lu_{1-x}Eu_xBO_3$, $Lu_{0.99-x}Tb_xEu_{0.01}BO_3$, and $Lu_{0.99-x}Y_xEu_{0.01}BO_3$ with $0 < x < 0.25$ synthesized at 970°C have been studied. An increase in x leads to a sequential change in the structural state of the orthoborates. At $x \le 0.07$–0.1, the compounds form the solid solution with the calcite structure and the microcrystal sizes 8–20 μm, then they become two-phase: the vaterite phase appears along with the calcite structure. At $x \ge 0.2$–0.25, a whole sample volume has the vaterite structure. It is found that there is correlation between the structure and the spectral characteristics of these compounds. The luminescence spectra are studied at various wavelengths of the exciting light, which allowed the obtainment of the information on the structure of the near- surface layer and the bulk of microcrystals of these samples. The vaterite phase is shown to form both in the coarse microcrystal bulks (8–20 μm), and as fine microcrystals (1–2 μm).

Keywords: luminophors for light-emitting diodes, rare-earth orthoborates, X-ray phase analysis, IR spectroscopy, luminescence spectra

DOI: 10.1134/S1063783421100346

1. INTRODUCTION

One of most efficient methods of the directional change in spectral characteristics of various polymorphic compounds of borates, molybdates, and tungstates containing optically active centers is a change in their structural states, since a rigidly certain luminescence spectrum corresponds to each structural modification [1–11]. The study of the method of directional controlling the spectral characteristics of rare-earth borates is of significant interest, since they can be used as efficient luminophors for LED light sources.

Significant changes in the spectral characteristics of Eu^{3+} ions in $REBO_3$ (Eu) compounds with a change the structural state of rare-earth borates allow one to use them as structure-sensitive and optically active marks. Since the spectral characteristics of Eu^{3+} ions are substantially dependent on their nearest surroundings [12, 13], then, as shown in [14–16], the sample is single-phase if the short-range order around Eu^{3+} ions is the same over entire sample volume, which is demonstrated by the coincidence of the luminescence spectra (LS) of the near-surface layer of the sample and its bulk.

As the luminescence of Eu^{3+} ions in $LuBO_3$ (Eu) orthoborates is excited by a light corresponding to the range of the intense absorption of the sample, for example, in the charge transfer band (CTB), λ_{ex} = 225–275 nm [2, 3, 14–17], we can obtain information on the local surroundings of the sample in the near-surface layer of the crystal. During the resonant excitation of the Eu^{3+} ion luminescence in the region of the crystal transparency (λ_{ex} ~ 394 and ~466 nm; electron transitions $^7F_0 \rightarrow {}^5L_6$ and $^7F_0 \rightarrow {}^5D_2$, respectively) [2, 3, 14–16], we obtain information on the nearest surroundings of Eu^{3+} ions in the crystal bulk. The study of the spectral characteristics of the near-surface layer and the crystal bulk allowed one to obtain the information on the structure on the surface and in bulk of microcrystals in solid solutions $Lu_{0.98-x}In_xEu_{0.02}BO_3$ and $Lu_{0.99-x}Gd_xEu_{0.01}BO_3$ [11, 18].

Lutetium borate ($LuBO_3$) has two stable structural modifications: vaterite (space group $C2/c$) which forms at the synthesis $LuBO_3$ at T = 750–850°C, and the calcite (space group $R\bar{3}c$) formed at T = 970–1100°C. The $REBO_3$ orthoborates, where RE = Eu, Gd, Tb, Dy, and Y have only one structural modification vaterite [19–21]. It is shown in [22, 23] that solid solutions $Lu_{1-x}RE_xBO_3$ (RE = Eu, Gd, Tb, Dy, and Y) at $x > 0.15$–0.2 synthesized at T = 970–1100°C (temperature of existing calcite phase $LuBO_3$) crystal-

lize in the vaterite structure. At the same time, it was established in [11] that solid solution $Lu_{1-x}In_xBO_3$ consisting of lutetium borate ($LuBO_3$), which has two stable structural modifications (vaterite and calcite) and indium orthoborate ($InBO_3$), which has only one structural modification (calcite) [24–26], synthesized at 780°C (temperature of existence of vaterite $LuBO_3$) at $x > 0.08$–0.1crystallizes in the calcite structure.

The studies of the luminescence of the $Lu_{0.98-x}In_xEu_{0.02}BO_3$ compounds when it was excited in the charge transfer band ($\lambda_{ex} = 250$ nm) and during the resonant excitation of Eu^{3+} ion ($\lambda_{ex} = 394$ nm) showed that the structural transformations in $Lu_{0.98-x}In_xEu_{0.02}BO_3$ orthoborates, as the In^{3+} ion concentration increases, start in a near-surface layer of microcrystals these samples [11]. At $x \geq 0.04$, the near-surface layer has the calcite structure; as the indium concentration increases, the calcite phase content increases also in the sample bulk; at $x > 0.1$, the entire sample has the calcite structure.

The studies of $Lu_{0.99-x}Gd_xEu_{0.01}BO_3$ orthoborates synthesized at 970°C showed that their structure is changed with an increase in the Gd concentration. At $0 \leq x \leq 0.05$, the solid solution of the orthoborates is single-phase and has the calcite structure (space group $R\bar{3}c$); at $0.05 < x \leq 0.1$, in addition to the calcite structure, the vaterite phase appears (space group $C2/c$) and, at $x > 0.1$, the solid solution is also single-phase with the vaterite structure (space group $C2/c$) [18]. The morphology of orthoborite microcrystals is also changed simultaneously with the structure. At $0 \leq x \leq 0.05$, there are coarse microcrystals (15–20 μm); in the Gd^{3+} ion concentration range $0.05 < x \leq 0.1$, in parallel with coarse microcrystals, fine microcrystals (1–2 μm) appear, the content of which increases with x; at $x > 0.1$, the 1–2 μm microcrystals dominate. It is shown in [18] that the 1–2 μm microcrystals have the vaterite structure (space group $C2/c$). Coarse microcrystals (15–20 μm) in the $Lu_{0.99-x}Gd_xEu_{0.01}BO_3$ orthoborates are two-phase at $0.05 < x \leq 0.1$. It is important to note that the vaterite phase reveals itself at $x > 0.05$ in the bulk of coarse nicrocrystals having the calcite structure and it appears also on their surface as the Gd^{3+} ion concentration increases further.

Thus, the formation of calcite in $Lu_{0.98-x}In_xEu_{0.02}BO_3$ microcrystals having the initial vaterite structure takes place first in near-surface regions of the sample as the In^{3+} ion concentration increases, while, in initial coarse $Lu_{0.99-x}Gd_xEu_{0.01}BO_3$ microcrystals having the calcite structure, vaterite forms, as the Gd^{3+} concentration increases, first in the bulks of these microcrystals.

It is important to establish how general is the structure transformation observed in the $Lu_{0.99-x}Gd_xEu_{0.01}BO_3$samples as the Gd^{3+} concentration increases. As was noted, in parallel with $GdBO_3$, orthoborates of some other rare-earth elements (Eu, Tb, Dy, Y, and other [19–21]) also have only one structural modification, namely, vaterite in the temperature range under study. This work is devoted to studies of the changes in the structure, the morphology, the IR absorption spectra, and also the luminescence excitation spectra and the luminescence of solid solutions $Lu_{1-x}RE_xBO_3$ (RE = Eu, Tb, and Y) with an increase in the RE concentration.

2. EXPERIMENTAL

2.1. Sample Synthesis

The samples of polycrystalline powders of lutetium orthoborate doped with Eu^{3+}, Tb^{3+}, and Y^{3+} were synthesized by interaction of rare-earth element oxides with a potassium tetraborate melt by the reaction

$$(1-x)Lu_2O_3 + xRE_2O_3 + K_2B_4O_7 = 2Lu_{1-x}RE_xBO_3 + K_2B_2O_4.$$

The potassium tetraborate amount taken into the reaction provided the excess of the boron-containing reagent with respect to the stoichiometric amount by 10–20%. The initial compounds for synthesizing lutetium orthoborate were potassium tetraborate $K_2B_4O_7 \cdot 4H_2O$, oxides Lu_2O_3, Eu_2O_3, Tb_2O_3, Y_2O_3, and nitric acid. All the chemical substances used in this work corresponded to analytic grade. Ions Lu^{3+}, Eu^{3+}, Tb^{3+}, and Y^{3+} were introduced to the reaction as aqueous solutions of their nitrate salts which were prepared by the dissolution of initial rare-earth oxides in nitric acid. The synthesis of the microcrystalline powders of lutetium orthoborate doped with Eu^{3+}, Tb^{3+}, and Y^{3+} was carried out as follows. A weighted amount of crystalline potassium tetraborate (hydrate) and the corresponding volume of the calibrated aqueous solution of rare-earth nitrides were placed into a ceramic cup and carefully mixed. The obtained aqueous suspension was heated on an electric stove and the water was removed during a careful boiling. The obtained solid product was annealed at 600°C for 20 min for removing the residual moisture and decomposing nitrate salts. The solid product–precursor was ground in an agate mortar, and the obtained powder was placed in a ceramic crucible 5 mL in volume or in a metallic cylindrical mold to form the powder as tablets 15 mm in diameter and 2.0–2.5 mm in thickness at a pressure of 5 kbar. Both precursors (the powder and the tablet) were subjected to high-temperature annealing at $T = 970$°C for 2 h. The obtained products were treated by the aqueous solution of hydrochloric acid with the concentration 5 wt % for 0.2 h. The separation of the orthoborate polycrystals were performed by filtering of the obtained aqueous suspension with subsequent washing with water, alcohol and drying the product on a filter. The obtained powders of orthoborate polycrystals were conclusively dried in air at $T = 200$°C for 0.5 h.

The products–precursors (the powder or the tablet) were pressed to elucidate the influence of their initial densities on the morphology of the obtained orthoborate microcrystals.

2.2. Methods of the Studies

X-ray diffraction studies were carried out on a Rigaku SmartLab SE diffractometer using the CuK_α radiation, $\lambda = 1.54178$ Å, 40 kV, 35 mA.The angular range is $2\theta = 10°–140°$. The phase analysis of the samples and the calculation of the lattice parameters were performed using the Match and PowderCell 2.4 programs.

The IR absorption spectra of the samples were measured on a VERTEX 80v Fourier spectrometer in the spectral range 400–5000 cm^{-1} with the resolution 2 cm^{-1}. For the measurements, the polycrystal powders were ground in an agate mortar and then deposited as a thin layer on the crystalline ground KBr substrate.

The morphology of the samples was studied using a Supra 50 VP X-ray microanalyzer with an adapter for EDS INCA (Oxford).

The photoluminescence spectra and the luminescence excitation spectra were studied on an installation consisting of a light source (DKSSh-150 lamp), two monochromators MDR-4 and MDR-6 (spectral range 200–1000 nm, dispersion 1.3 nm/mm). The luminescence was registered by a FEU-106 photomultiplier (the spectral sensitivity range is 200–800 nm) and am amplifying system. The MDR-4 monochromator was used for studying the luminescence excitation of the samples, and the MDR-6 monochromator was used for studying the luminescence spectra.

The spectral and structural characteristics, and also the morphology of the samples were studied at room temperature.

3. X-RAY DIFFRACTION STUDIES

Figure 1 shows the X-ray diffraction patterns of the powder samples of the $Lu_{1-x}RE_xBO_3$ (RE = Eu, Tb, and Y) compounds. The phase compositions of the samples are given in Table 1. Orthoborates $Lu_{1-x}Eu_xBO_3$ at $0 \le x \le 0.07$, $Lu_{0.99-x}Tb_xEu_{0.01}BO_3$ at $0 \le x \le 0.09$, and $Lu_{0.99-x}Y_xEu_{0.01}BO_3$ at $0 \le x \le 0.10$ are single-phase and have the calite structure (PDF 72-1053), i.e., the rhombohedral $R\bar{3}c$ structure (space group no. 167), $Z = 6$. Solid solutions $Lu_{1-x}Eu_xBO_3$ at $0.07 < x < 0.2$, $Lu_{0.99-x}Tb_xEu_{0.01}BO_3$ at $0.09 < x < 0.2$, and $Lu_{0.99-x}Y_xEu_{0.01}BO_3$ at $0.1 < x < 0.25$ are two-phase: in parallel to the calcite structure, the vaterite phase is observed: monoclinic, $C2/c$ (space group no. 15), $Z = 12$ [27]. As seen from Table 1, the vaterite phase content increases with the concentration of RE^{3+} ions. Compounds $Lu_{1-x}Eu_xBO_3$ and $Lu_{0.99-x}Tb_xEu_{0.01}BO_3$ at $x \ge 0.2$, and $Lu_{0.99-x}Y_xEu_{0.01}BO_3$ at $x \ge 0.25$ becomes single-phase once again and have the vaterite structure (Table 1).

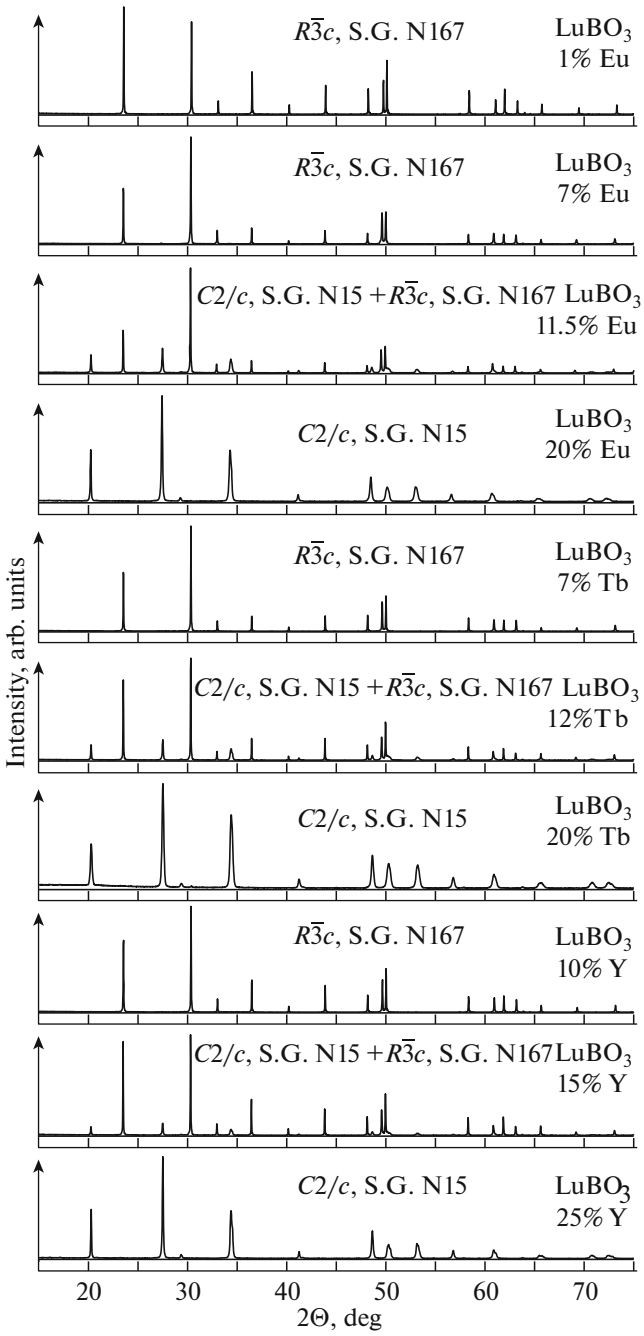

Fig. 1. X-ray diffraction patterns of the $Lu_{1-x}RE_xBO_3$ (RE = Eu, Tb, and Y) samples ($0 \le x \le 0.25$).

Thus, in orthoborates $Lu_{1-x}RE_xBO_3$ (RE = Eu, Tb, and Y), as well as in the $Lu_{0.99-x}Gd_xEu_{0.01}BO_3$ compounds, we can separate three ranges of the RE concentrations, in which there are certain structural states. As the RE concentration increases, the sequential change of two types of the crystalline phases takes

Table 1. Effect of the RE^{3+} concentration on the content of calcite and vaterite phases in orthoborates $Lu_{1-x}RE_xBO_3$ (RE = Eu, Tb, and Y)

$Lu_{1-x}RE_xBO_3$ (RE = Eu, Tb, Y) RE, at %	Calcite phase (S.G. no. 167), %	Vaterite phase (S.G. no. 15), %
Eu, 1	100	0
Eu, 7	100	0
Eu, 9	86.5	13.5
Eu, 11.5	36	64
Eu, 15	4	96
Eu, 20	0	100
Tb, 7	100	0
Tb, 9.5	96.5	3.5
Tb, 10.5	79	21
Tb, 12	72	28
Tb, 15	14	86
Tb, 20	0	100
Y, 10	100	0
Y, 15	80	20
Y, 20	10	90
Y, 25	0	100
*Eu, 9	100	0
*Eu, 15	25	75
**Tb, 14	39	61
**Tb, 16	0	100
*Y, 15	52	48
*Y, 20	4.5	95.5

*Samples subjected to pressing before annealing.
**The data of [10].

place. First, solid solution $Lu_{1-x}RE_xBO_3$ (RE = Eu, Tb, and Y) has the calcite structure; then, as the RE concentration increases, the $Lu_{1-x}RE_xBO_3$ compound becomes two-phase: the vaterite phase appears in addition to the calcite structure; at further increase in the RE concentration, the solid solution has the vaterite structure (Table 2).

It is important to note that the concentration ranges of doping rare-earth elements (x), at which the structural states are changed, are noticeably larger in orthoborites $Lu_{1-x}RE_xBO_3$ (RE = Eu, Tb, and Y) than in $Lu_{0.99-x}Gd_xEu_{0.01}BO_3$ (Table 2).

Figure 2 demonstrates the change in the phase composition of $Lu_{1-x}Eu_xBO_3$ as the Eu^{3+} concentration increases. As seen from Fig. 2, the solubility limit of Eu^{3+} ions in the calcite (rhombohedral) modification of $LuBO_3$ is ~7 at %, and the solubility limit of Lu^{3+} ions in the vaterite (monoclinic) modification of $EuBO_3$ is ~80 at %. Similar dependences of the changes in the phase compositions were obtained for ortoborates $Lu_{0.99-x}Tb_xEu_{0.01}BO_3$ and $Lu_{0.99-x}Y_xEu_{0.01}BO_3$. The solubility limits of Tb^{3+} and Y^{3+} ions in the rhombohedral modification of $LuBO_3$ are ~9 and 10 at %, respectively, and the solubility limit of Lu^{3+} ions in the monoclinic modifications of $TbBO_3$ and YBO_3 are ~80 and 75 at %, respectively. The significant differences in the solubility limits of ions Eu^{3+}, Tb^{3+}, and Y^{3+} in $LuBO_3$ and ions Lu^{3+} in $EuBO_3$, $TbBO_3$, and YBO_3 are related to the fact that the Lu^{3+} ion radius (0.867 Å) is markedly smaller than the ionic radii of ions Eu^{3+} (0.987 Å), Tb^{3+} (0.956 Å), and Y^{3+} (0.928 Å) [28]

It should be noted that we observed similar changes in the phase compositions in molibdates $(Lu_{1-x}Eu_x)_2(MoO_4)_3$ and tungstates $(Lu_{1-x}Eu_x)_2(WO_4)_3$ [29, 30].

4. MORPHOLOGY OF THE SAMPLES

4.1. Morphology of Orthoborates $Lu_{1-x}Eu_xBO_3$ and $Lu_{0.99-x}Tb_xEu_{0.01}BO_3$

In the $Lu_{1-x}Eu_xBO_3$ and $Lu_{0.99-x}Tb_xEu_{0.01}BO_3$ samples, in the range of concentration of Eu^{3+} $0 \le x \le 0.07$ and Tb^{3+} $0 \le x \le 0.09$, respectively, which have, according to the data of the X-ray analysis, the calcite structure (Table 1), there are coarse microcrystals with sizes ~15–20 μm (Figs. 3a, 3f). As the europium

Table 2. RE concentration regions, in which there are certain structural states of orthoborate $Lu_{1-x}RE_xBO_3$ (RE = Eu, Tb, and Y)

Compound	The values of x, at which there are the structures noted		
	Calcite ($R\bar{3}c$)	Calcite ($R\bar{3}c$) + vaterite ($C2/c$)	Vaterite ($C2/c$)
$Lu_{1-x}Eu_xBO_3$	$0 \le x \le 0.07$	$0.07 < x < 0.2$	$x \ge 0.2$
$Lu_{0.99-x}Tb_xEu_{0.01}BO_3$	$0 \le x \le 0.09$	$0.09 < x < 0.2$	$x \ge 0.2$
$Lu_{0.99-x}Y_xEu_{0.01}BO_3$	$0 \le x \le 0.10$	$0.1 < x < 0.25$	$x \ge 0.25$
*$Lu_{0.99-x}Gd_xEu_{0.01}BO_3$	$0 \le x \le 0.05$	$0.05 < x \le 0.1$	$x > 0.1$

* Data from [18].

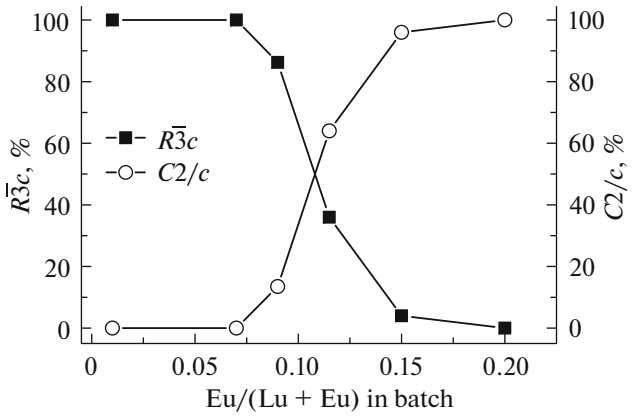

Fig. 2. Phase composition of the synthesized $Lu_{1-x}RE_xBO_3$ as a function of the ratio of rare-earth elements in the batch at $0 \le x \le 0.2$.

(terbium) concentration increases, fine 1–2 μm microcrystals appear in addition to the coarse microcrystals. As the concentration of $Eu^{3+}(Tb^{3+})$ ions increases, the amount of the fine microcrystal increases and that of coarse microcrystals decreases; in this case, the amount of the vaterite phase increases (Figs. 3b, 3c, 3g, 3h, and 3k). In the samples $Lu_{0.8}Eu_{0.2}BO_3$ and $Lu_{0.79}Tb_{0.2}Eu_{0.01}BO_3$ having the vaterite structure (Table 1), there is majority of fine microcrystals (Figs. 3d and 3l).

Thus, based on the studies of the phase compositions of the $Lu_{0.8}Eu_{0.2}BO_3$ and $Lu_{0.79}Tb_{0.2}Eu_{0.01}BO_3$ samples, it can be assumed that the 1–2 μm microcrystals in $Lu_{1-x}Eu_xBO_3$ and $Lu_{0.99-x}Tb_xEu_{0.01}BO_3$, as well as in the $Lu_{0.99-x}Gd_xEu_{0.01}BO_3$ [18] compounds, have the vaterite structure.

The estimation of the ratios of the volumes of fine and coarse microcrystals in Figs. 3b, 3c, 3h, 3k, and 3l (in samples $Lu_{0.91}Eu_{0.09}BO_3$, $Lu_{0.885}Eu_{0.115}BO_3$, $Lu_{0.87}Tb_{0.12}Eu_{0.01}BO_3$, and $Lu_{0.84}Tb_{0.15}Eu_{0.01}BO_3$) showed that the content of fine microcrystals in the vaterite phase is ~0.4, 6–7, 3–4, and 13–14%, respectively. At the same time, according to the data of the X-ray phase analysis, the vaterite phase content in these samples is significantly higher, namely, 13.5, 64, 28, and 86%, respectively (Table 1). This fact shows that the coarse microcrystals (15–20 μm) in compounds $Lu_{1-x}Eu_xBO_3$ at $0.07 < x < 0.2$ and $Lu_{0.99-x}Tb_xEu_{0.01}BO_3$ at $0.09 < x < 0.2$, as well as in samples $Lu_{0.99-x}Gd_xEu_{0.01}BO_3$ at $0.05 < x \le 0.1$ are two-phase and contain the vaterite and calcite phases.

It should be noted that the ratio of the contents of fine and coarse microcrystals is substantially dependent on the method of synthesizing the samples. If the batch was subjected to pressing before annealing at 970°C, then, in the $*Lu_{0.85}Eu_{0.15}BO_3$, $*Lu_{0.85}Tb_{0.14}Eu_{0.01}BO_3$, and $*Lu_{0.83}Tb_{0.16}Eu_{0.01}BO_3$ samples containing 75, 61%, and 100% vaterite, respectively, the majority of microcrystals have size 8–12 μm and the content of fine 1–2-μm microcrystals is lower by many times than in the samples which were not subjected to the preliminary pressing (Figs. 3e, 3m, and 3n). This fact shows that, in the $*Lu_{0.85}Eu_{0.15}BO_3$ and $*Lu_{0.85}Tb_{0.14}Eu_{0.01}BO_3$ compounds obtained after annealing at 970°C of pressed tablets, microcrystals with sizes 8–12 μm are two-phase. At $x \ge 0.16$, 8–12-μm microcrystals in $*Lu_{0.99-x}Tb_xEu_{0.01}BO_3$ have the vaterite structure (Fig. 3n), while, in the $Lu_{0.99-x}Tb_xEu_{0.01}BO_3$ samples, which were not pressed preliminarily, the 1–2-μm microcrystals have the vaterite structure after annealing at 970°C (Fig. 3l).

4.2. Morphology of Orthoborates $Lu_{0.99-x}Y_xEu_{0.01}BO_3$

The $Lu_{0.99-x}Y_xEu_{0.01}BO_3$ orthoborates samples at $0 \le x \le 0.1$, which have the calcite structure, according to the X-ray phase analysis data (Table 1), consist of coarse ~15–20-μm microcrystals (Fig. 4a). At $x > 0.1$, the 8–18-μm microcrystals are mainly observed, and the volume of the fine 1–2-μm microcrystals is many times smaller than that of the coarse microcrystals (Figs. 4b, 4c, and 4d). The largest amount of the 1–2-μm microcrystals is observed in the $Lu_{0.84}Y_{0.15}Eu_{0.01}BO_3$ samples (Fig. 4b). The estimation of the ratio of the volumes of the fine and coarse microcrystals in these samples in Fig. 4b shows that the content of the fine microcrystals, which are in the vaterite phase, is ~1% even in these samples. At the same time, according to the X-ray phase analysis data, the content of the vaterite phase in these samples is significantly higher and is 20% (Table 1). This fact shows that coarse 8–18-μm microcrystals in the $Lu_{0.84}Y_{0.15}Eu_{0.01}BO_3$ compound are two-phase and contain the vaterite and calcite phases.

According to the X-ray phase analysis data, at $0.1 < x < 0.25$, the $Lu_{0.99-x}Y_xEu_{0.01}BO_3$ compounds are two-phase; therefore, the microcrystals (8–18 μm) of these compounds are also two-phase. At $x \ge 0.25$, the $Lu_{0.99-x}Y_xEu_{0.01}BO_3$ samples have a vaterite structure (Table 1); therefore, microcrystals 8–20 μm in size are single-phase and have a vaterite structure. In these microcrystals, there are many distortions of continuity in the crack form (Figs. 4a, 4d, and 4e).

It should be noted that, unlike on orthoborates $Lu_{1-x}Eu_xBO_3$ and $Lu_{0.99-x}Tb_xEu_{0.01}BO_3$, the pressing of the $Lu_{0.99-x}Y_xEu_{0.01}BO_3$ tablets before annealing at 970°C only slightly influences the morphology of these samples. In the $Lu_{0.99-x}Y_xEu_{0.01}BO_3$ samples with $0.1 < x \le 0.2$, which were subjected to pressing before the annealing, the 8–20 μm microcrystals are observed, and the content of fine microcrystals is much lower (Figs. 4f, 4g, and 4h). At $0.1 < x < 0.2$, according to the X-ray phase analysis data, the 8–20-μm microcrystals are two-phase (Table 1). It

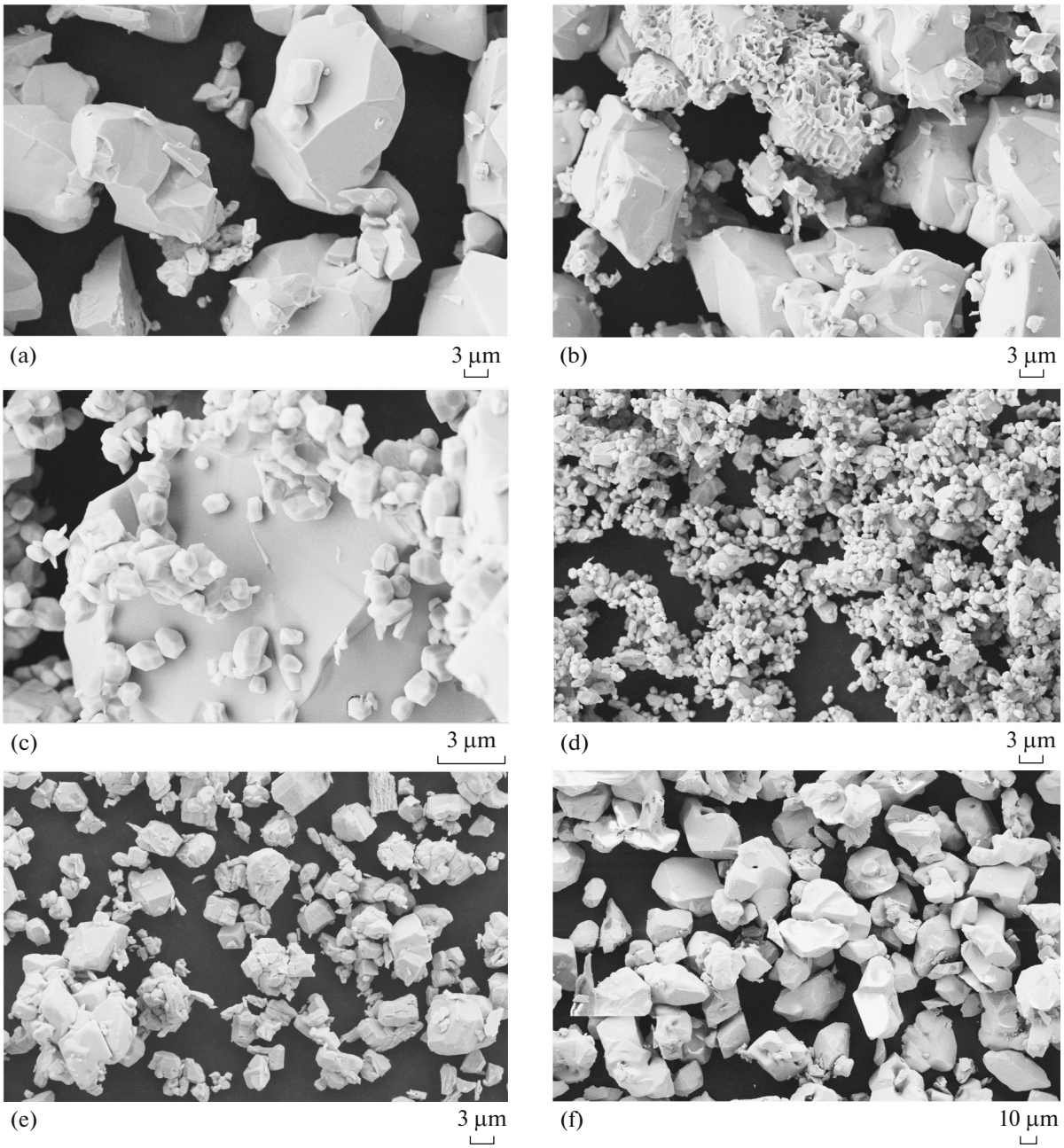

Fig. 3. Morphology of $Lu_{1-x}Eu_xBO_3$ and $Lu_{0.99-x}Tb_xEu_{0.01}BO_3$: (a) $Lu_{0.93}Eu_{0.07}BO_3$, (b) $Lu_{0.91}Eu_{0.09}BO_3$, (c) $Lu_{0.885}Eu_{0.115}BO_3$, (d) $Lu_{0.8}Eu_{0.2}BO_3$, (e) $*Lu_{0.85}Eu_{0.15}BO_3$, (f) $Lu_{0.92}Tb_{0.07}Eu_{0.01}BO_3$, (g) $Lu_{0.885}Tb_{0.105}Eu_{0.01}BO_3$, (h) $Lu_{0.87}Tb_{0.12}Eu_{0.01}BO_3$, (k) $Lu_{0.84}Tb_{0.15}Eu_{0.01}BO_3$, (l) $Lu_{0.79}Tb_{0.2}Eu_{0.01}BO_3$, (m) $*Lu_{0.85}Tb_{0.14}Eu_{0.01}BO_3$, (n) $*Lu_{0.83}Tb_{0.16}Eu_{0.01}BO_3$ ((e, m, and n) are the samples subjected to pressing before annealing).

should be noted that these microcrystals have numerous cracks and defects (Figs. 4f, 4g, and 4h).

Thus, the morphology of orthoborates $Lu_{0.99-x}Y_xEu_{0.01}BO_3$ noticeably differs from the morphologies of the $Lu_{1-x}Eu_xBO_3$ and $Lu_{0.99-x}Tb_xEu_{0.01}BO_3$ compounds. The $Lu_{0.99-x}Y_xEu_{0.01}BO_3$ samples having the vaterite structure consist mainly of the 8–20 μm microcrystals, while the $Lu_{1-x}Eu_xBO_3$ and $Lu_{0.99-x}Tb_xEu_{0.01}BO_3$ samples with the vaterite structure consists of the 1–2-μm microcrystals.

5. RESULTS OF THE IR SPECTROSCOPIES

Figure 5 shows the IR absorption spectra of the compounds $Lu_{0.99-x}Eu_xBO_3$ ($0.01 \le x \le 0.2$), $Lu_{0.99-x}Tb_xEu_{0.01}BO_3$ ($0.07 \le x \le 0.2$), and

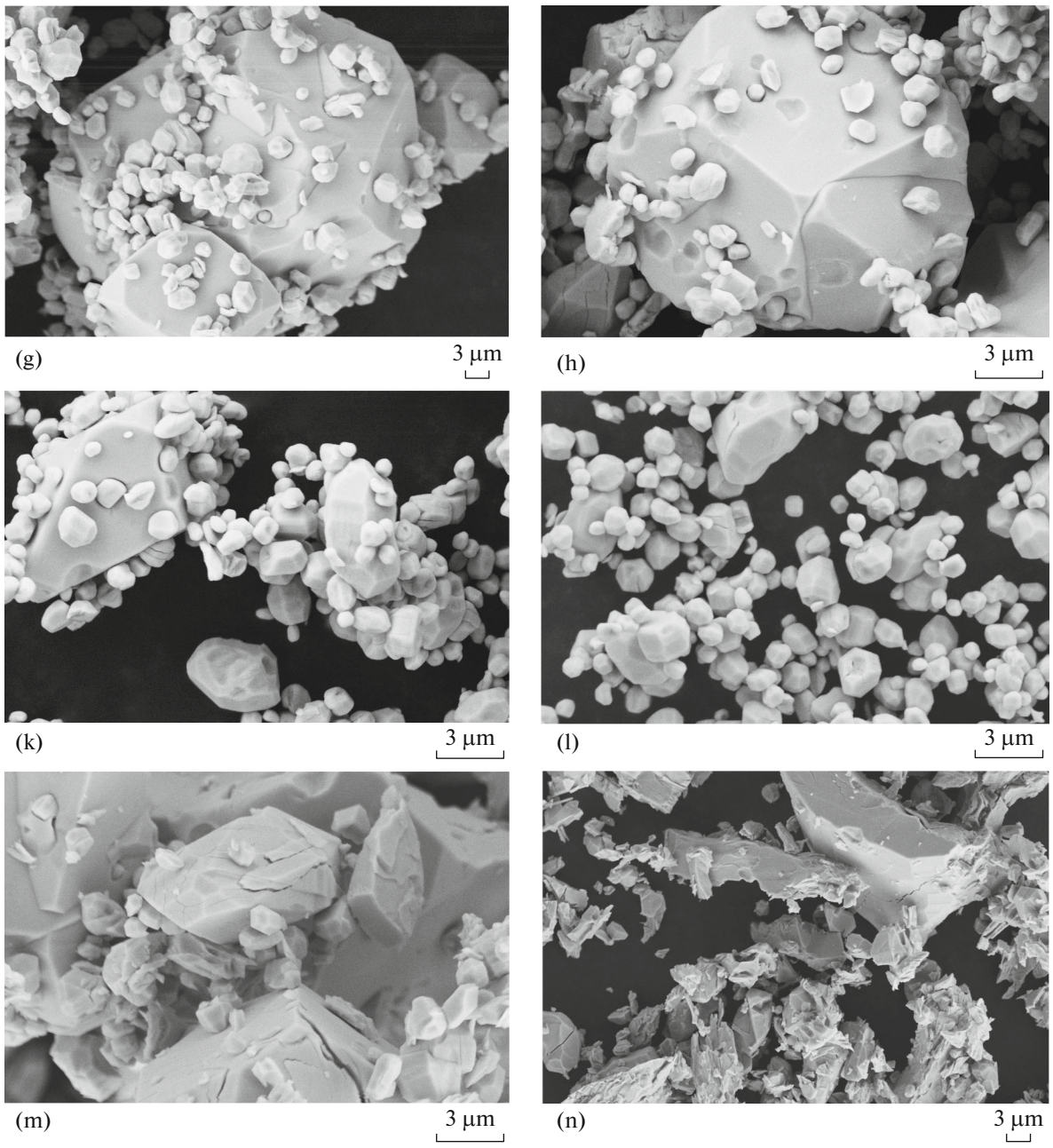

Fig. 3. (Contd.)

$Lu_{0.99-x}Y_xEu_{0.01}BO_3$ ($0.1 \le x \le 0.25$) [23, 31, 32]. The spectra of orthborates $Lu_{0.99}Eu_{0.01}BO_3$, $Lu_{0.92}Tb_{0.07}Eu_{0.01}BO_3$, and $Lu_{0.89}Y_{0.10}Eu_{0.01}BO_3$ (Fig. 5, spectra *1*, *4*, and *7*), which have the calcite structure and are single phase, according to the X-ray phase analysis data (Table 1), have the IR absorption bands near 1230, 770, 740, and 630 cm^{-1} due to the B–O bond vibrations in the structure with the trigonal coordination of boron atoms characteristic of the calcite phase [23, 31, 32]. The $Lu_{0.8}Eu_{0.2}BO_3$, $Lu_{0.79}Tb_{0.2}Eu_{0.01}BO_3$, and $Lu_{0.74}Y_{0.25}Eu_{0.01}BO_3$ samples have the vaterite structure (Table 1). The IR spectra of these samples (Fig. 5, spectra *3*, *6*, and *9*) contain the absorption bands near 570, 720, 880, 940, 1040, and 1100 cm^{-1} characteristic of the samples with the vaterite structure, in which boron atoms have the tetrahedral coordination of atoms [3, 23, 31, 32].

In these spectra, the absorption bands are also due to the B–O bond vibrations. They were observed repeatedly in the spectra of orthoborates of various rare-earth elements (Gd, Er, Dy, Ho, Yb, and Y) with the vaterite structure [33–35]. The IR spectra of

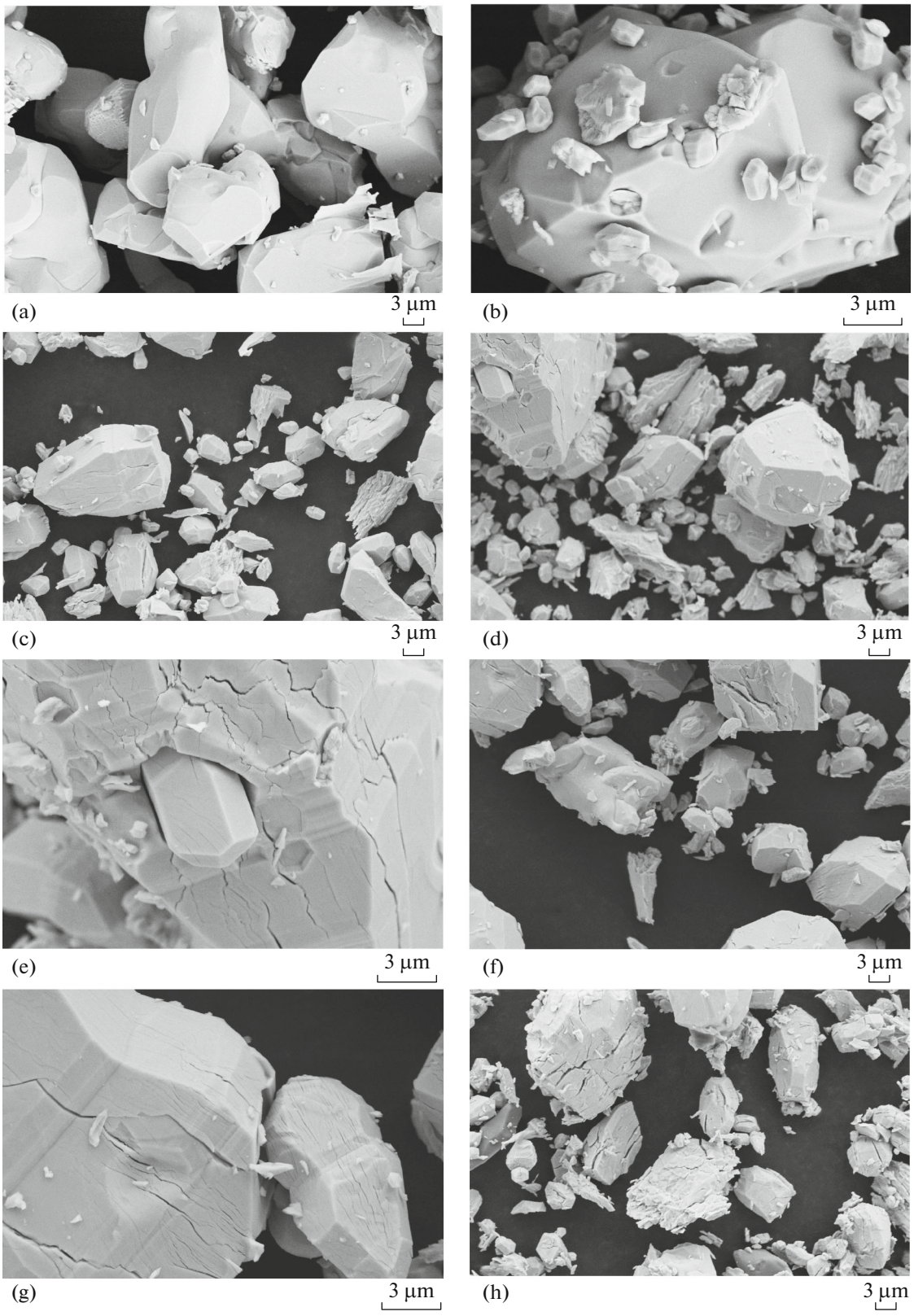

Fig. 4. Morphology of $Lu_{0.99-x}Y_xEu_{0.01}BO_3$ samples: (a) $Lu_{0.89}Y_{0.1}Eu_{0.01}BO_3$, (b) $Lu_{0.84}Y_{0.15}Eu_{0.01}BO_3$, (c) $Lu_{0.79}Y_{0.2}Eu_{0.01}BO_3$, (d) $Lu_{0.74}Y_{0.25}Eu_{0.01}BO_3$, (e) $Lu_{0.74}Y_{0.25}Eu_{0.01}BO_3$, (f) *$Lu_{0.84}Y_{0.15}Eu_{0.01}BO_3$, (g) *$Lu_{0.84}Y_{0.15}Eu_{0.01}BO_3$, (h) *$Lu_{0.79}Y_{0.2}Eu_{0.01}BO_3$ (f, g, and h) are the samples subjected to pressing before annealing.

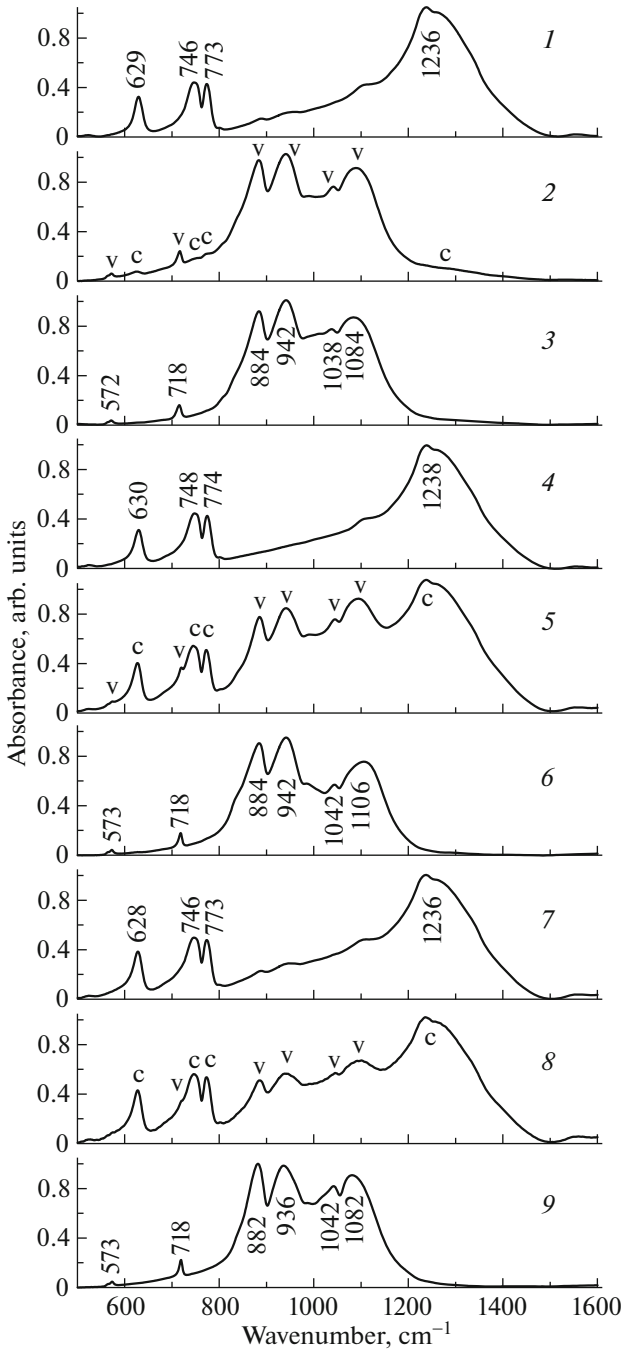

Fig. 5. IR absorption spectra of orthoborates: (*1*) $Lu_{0.99}Eu_{0.01}BO_3$, (*2*) $Lu_{0.8}Eu_{0.2}BO_3$, (*3*) $Lu_{0.85}Eu_{0.15}BO_3$, (*4*) $Lu_{0.92}Tb_{0.07}Eu_{0.01}BO_3$, (*5*) $Lu_{0.79}Tb_{0.2}Eu_{0.01}BO_3$, (*6*) $Lu_{0.87}Tb_{0.12}Eu_{0.01}BO_3$, (*7*) $Lu_{0.89}Y_{0.10}Eu_{0.01}BO_3$, (*8*) $Lu_{0.74}Y_{0.25}Eu_{0.01}BO_3$, and (*9*) $Lu_{0.84}Y_{0.15}Eu_{0.01}BO_3$.

orthoborates $Lu_{0.85}Eu_{0.15}BO_3$, $Lu_{0.87}Tb_{0.12}Eu_{0.01}BO_3$, and $Lu_{0.84}Y_{0.15}Eu_{0.01}BO_3$ correspond to the two-phase state of these compounds and include the absorption bands of calcite (*c*) and vaterite (*v*) (Fig. 5, spectra *2*, *5*, and *8*). As was established by the X-ray phase analysis, the calcite/vaterite phase ratios in these samples are 4/96, 72/28, and 80/20%, respectively (Table 1). These phase ratios agree well with the ratios of the intensities of the corresponding absorption bands of the *c* and *v* phases in the IR spectra (Fig. 5, spectra *2*, *5*, and *8*).

6. LUMINESCENCE SPECTRA AND LUMINESCENCE EXCITATION SPECTRA

The luminescence spectra of the Eu^{3+} ions in the $LuBO_3$(Eu) samples having the calcite structure contain two narrow bands with $\lambda_{max} = 589.8$ and 595.7 nm (the $^5D_0 \rightarrow {}^7F_1$ electron transition) [2, 22, 23]. The luminescence spectra of the Eu^{3+} ions in the vaterite modification $REBO_3$(Eu), where RE = Lu, Tb, Y, and Gd, contains three bands in the wavelength region 588–596 nm (the $^5D_0 \rightarrow {}^7F_1$ electron transition), 608–613 nm and 624–632 nm ($^5D_0 \rightarrow {}^7F_2$) [2–4, 22]. According to the X-ray phase analysis data, orthoborates $Lu_{1-x}Eu_xBO_3$ at $0 \le x \le 0.07$, $Lu_{0.99-x}Tb_xEu_{0.01}BO_3$ at $0 \le x \le 0.09$ and $Lu_{0.99-x}Y_xEu_{0.01}BO_3$ at $0 \le x \le 0.1$ have the calcite structure. The $Lu_{1-x}Eu_xBO_3$ and $Lu_{0.99-x}Tb_xEu_{0.01}BO_3$ have the vaterite structure at $x \ge 0.2$ and $Lu_{0.99-x}Y_xEu_{0.01}BO_3$, at $x \ge 0.25$ (Table 1).

In this work, the Eu^{3+} ions with concentration 1 at % were used as optically active and structurally sensitive marks in the samples of the lutetium borates doped with Tb and Y.

6.1. The Luminescence Excitation Spectra of Orthoborates

The spectrum of the excitation of the most intense luminescence band of Eu^{3+} ions in the calcite modification $Lu_{1-x}Eu_xBO_3$ ($\lambda_{max} = 589.8$ nm) of lutetium borate at $x = 0.07$ is shown in Fig. 6, spectrum *1*. Similar spectra are observed for $Lu_{1-x}Eu_xBO_3$ at $0 \le x \le 0.07$. The luminescence excitation spectra of bands at $\lambda_{max} = 589.8$ and 595.7 nm coincide. In the luminescence excitation spectra (LES) of the $Lu_{1-x}Eu_xBO_3$ at $0 \le x \le 0.07$ obtained at 970°C, there are a broad short-wave band at wavelengths 220–290 nm ($\lambda_{ex} \sim 260$ nm) (the charge transfer band) and a number of narrow bands in the wavelength range 290–500 nm (Fig. 6, spectrum *1*). In this spectral range, the band corresponding to the resonant excitation of Eu^{3+} ions ($\lambda_{ex} = 394$ nm ($^7F_0 \rightarrow {}^5L_6$)) is the most intense. The charge transfer band intensity is higher by a factor of ~10 than the intensity of the band with $\lambda_{ex} = 394$ nm. The existence of the dominating short-wave band is an important feature of LES of the samples with the calcite structure. Another situation is observed in the $Lu_{1-x}Eu_xBO_3$ samples with the vaterite structure.

LES of the most intense luminescence band of Eu^{3+} ions (λ_{max} = 593.3 nm) in lutetium borate doped with 20 at % Eu with the vaterite structure (Table 1) also contains the broad short-wave charge transfer band with a maximum at ~247 nm and a number of narrow resonant bands, from which the most intense band is at λ_{ex} = 394 nm, and also there are bands at ~467 and 469 nm ($^7F_0 \rightarrow {}^5D_2$) (Fig. 6, spectrum *2*). In the samples containing 20 at % Eu, the intensity of the resonant band at 394 nm is higher by a factor of ~1.6 than that of the charge transfer band.

The luminescence excitation spectra of main luminescence bands of orthoborates $Lu_{0.99-x}Y_xEu_{0.01}BO_3$ are similar to LES of the $Lu_{1-x}Eu_xBO_3$ compounds (Fig. 6, spectra *3* and *4*). In the luminescence excitation spectra of the most intense luminescence band of the calcite modification of the $Lu_{0.89}Y_{0.1}Eu_{0.01}BO_3$ samples (λ_{max} = 589.8 nm), the ultraviolet band (charge transfer band) ~250 nm has the highest intensity (Fig. 6, spectrum *3*). The intensity of the resonant band corresponding to the excitation of Eu^{3+} ions (394 nm) is more than 30 times lower than the CTB intensity. The luminescence excitation spectrum of the band with λ_{max} = 593.3 nm for $Lu_{0.74}Y_{0.25}Eu_{0.01}BO_3$ samples with a vaterite structure (Table 1) contains a broad short-wave band (CTB) with a maximum at ~243 nm and a number of narrow resonant bands, from which the most intense band is at 394 nm (Fig. 6, spectrum *4*). It is important to note that the CTB intensity in the vaterite modification of lutetium borate doped with 25 at % Y higher than the intensity of the resonant excitation band of Eu^{3+} ions (394 nm) by a factor of only ~1.2.

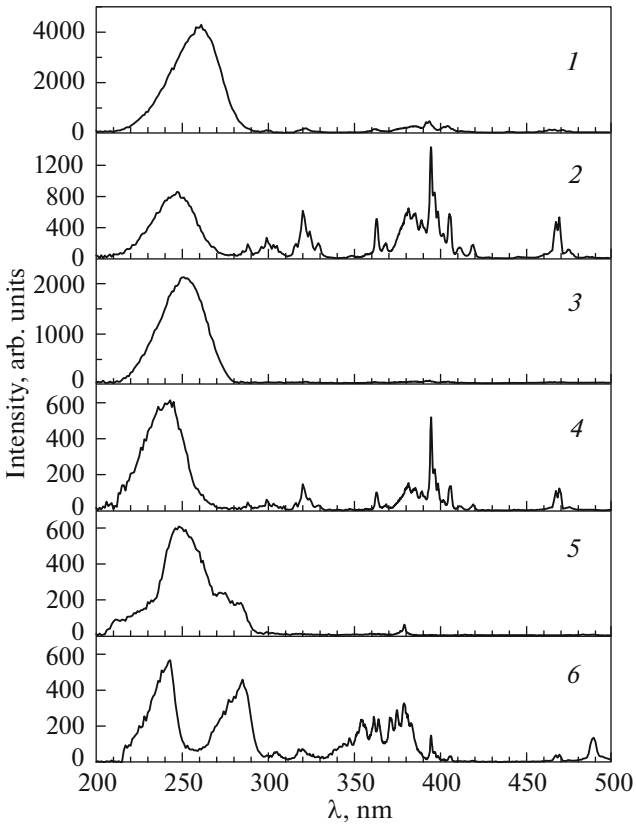

Fig. 6. Luminescence excitation spectra of orthoborates: (*1*) $Lu_{0.93}Eu_{0.07}BO_3$, (*2*) $Lu_{0.8}Eu_{0.2}BO_3$, (*3*) $Lu_{0.89}Y_{0.1}Eu_{0.01}BO_3$, (*4*) $Lu_{0.74}Y_{0.25}Eu_{0.01}BO_3$, (*5*) $Lu_{0.92}Tb_{0.07}Eu_{0.01}BO_3$, (*6*) $Lu_{0.79}Tb_{0.2}Eu_{0.01}BO_3$. (*1*, *3*, *5*) λ_{max} = 589.8 nm; (*2*, *4*, *6*) λ_{max} = 593.3 nm.

As the luminescence of Eu^{3+} ions is excited by a light corresponding to the range of the intense absorption of the sample (in the charge transfer band), we obtain information on the nearest surroundings of the Eu^{3+} ions in a near-surface layer of microcrystals in the sample. As the luminescence of the sample is excited in the transparence range (λ = 300–500 nm), we obtain information on the nearest surroundings of Eu^{3+} ions in the bulk of microcrystals of the sample.

In the luminescence excitation spectrum (LES) of the most intense luminescence band of Eu^{3+} ions in the calcite modification of orthoborate $Lu_{0.92}Tb_{0.07}Eu_{0.01}BO_3$ (λ_{max} = 589.8 nm), we observe a broad band in the wavelength range 220–290 nm (charge transfer band), a narrow band with λ_{ex} = 378 nm, and a very weak resonant excitation band of Eu^{3+} ions λ_{ex} = 394 nm (Fig. 6, spectrum *5*). It should be noted that the band at 378 nm is observed in LES of the most intense luminescence band of Tb^{3+} ions in the $Lu_{0.95}Tb_{0.05}BO_3$) samples having the calcite structure λ_{max} = 541.8 nm) ($^5D_4 \rightarrow {}^7F_5$)). In addition to the band at 378 nm, the LEC of Tb^{3+} ions contains still four bands in the short-wave spectral range with λ_{ex} = 235, 260.2, 273.5, and 284.3 nm (the $4f^8 \rightarrow 4f^75d^1$ transition) [3, 4, 23].

It is important to note that, when exciting Tb^{3+} ions in the $Lu_{0.92}Tb_{0.07}Eu_{0.01}BO_3$ samples (λ_{ex} = 378 nm ($^7F_6 \rightarrow {}^5D_3$)), the luminescence of Eu^{3+} ions is observed, which demonstrates unambiguously on the energy transfer from Tb^{3+} ions to Eu^{3+} ions. The short-wave bands observed in LES of Tb^{3+} ions have the form of weak peculiarities in the charge transfer band in LES of Eu^{3+} ions (Fig. 6, spectrum *5*). The intensity of the resonant luminescence excitation band of Eu^{3+} ions (λ_{ex} = 394 nm) is ~40 times lower than that of CTB, while the intensity of the band at 378 nm is ~10 times lower than the CTB intensity.

The luminescence excitation spectrum of the most intense luminescence band of Eu^{3+} ions in the vaterite modification of orthoborate $Lu_{0.79}Tb_{0.2}Eu_{0.01}BO_3$ (λ_{max} = 593.3 nm) is shown in Fig. 6 (spectrum *6*). In the LES, there are two broad short-wave bands with λ_{ex} = 242 and 285 nm and a number of narrow bands in the wavelength range 360–390 nm from which the band at 378 nm is the most intense. Moreover, in the

LES of $Lu_{0.79}Tb_{0.2}Eu_{0.01}BO_3$, there is resonant luminescence excitation band of Eu^{3+} ions (λ_{ex} = 394 nm) and also the bands at 467, 469 nm ($^7F_0 \rightarrow {}^5D_2$), and 489 nm. The excitation spectrum of the most intense luminescence band of Tb^{3+} ions in the $Lu_{0.8}Tb_{0.2}BO_3$ samples having the vaterite structure (λ_{max} = 542.3 nm) ($^5D_4 \rightarrow {}^7F_5$)) have the bands at 242 nm and 285 nm (transition $4f^8 \rightarrow 4f^75d^1$), narrow bands in the range 360–390 nm, bands 378 and 489 nm ($^7F_6 \rightarrow {}^5D_4$) [3, 4, 23]. Thus, in the vaterite structure of orthoborates $Lu_{0.79}Tb_{0.2}Eu_{0.01}BO_3$, as well as in the calcite modification, the luminescence of Eu^{3+} ions is observed during the excitation of Tb^{3+} ions (λ_{ex} = 242, 285, 378, and 489 nm), which demonstrates the energy transfer from Tb^{3+} ions to Eu^{3+} ions. For the calcite and vaterite modifications of $Lu_{0.99-x}Tb_xEu_{0.01}BO_3$, the Eu^{3+} ion luminescence intensity, in the case of excitation by the light with λ_{ex} = 378 nm, is several times higher than that at the resonant escitation of Eu^{3+} (λ_{ex} = 394 nm). Thus, to obtain information on the nearest surroundings of Eu^{3+} ions located in the bulk of these samples, the Eu^{3+} ion luminescence spectra will be studied at λ_{ex} = 378 nm.

It should be noted that the intensity of the 242-nm band (I_{242}) in the LES of Tb^{3+} ions in the $Lu_{0.8}Tb_{0.2}BO_3$ samples is lower than the 285-nm band intensity (I_{285}) by a factor of 1.3 [23]. At the same time, I_{242} in the LES of Eu^{3+} ions in $Lu_{0.79}Tb_{0.2}Eu_{0.01}BO_3$ is higher than I_{285} by a factor of 1.24 (Fig. 6, spectrum *6*). The increase in the intensity of the band at 242 nm by a factor of 1.6 in the $Lu_{0.79}Tb_{0.2}Eu_{0.01}BO_3$ samples is most likely due to the superposition of the 242-nm band and the charge transfer band disposed in the same wavelength range.

Based on the studies of the luminescence excitation spectra of Eu^{3+} ions in the $Lu_{0.99-x}Tb_xEu_{0.01}BO_3$ sample, the following conclusion can be made. The information on the nearest surroundings of Eu^{3+} ions in a near-surface layer and in the bulk of the sample can be obtained exciting the luminescence of Eu^{3+} ions by the light with λ_{ex} = 250–240 nm and 378 nm, respectively.

6.2. Luminescence Spectra of Orthoborates $Lu_{1-x}Eu_xBO_3$ and $Lu_{0.99-x}Tb_xEu_{0.01}BO_3$

Figure 7 shows the luminescence spectra (LS) of $Lu_{1-x}Eu_xBO_3$ (x = 0.07, 0.09, 0.115, 0.15, and 0.2) compounds excited by the light (λ_{ex} = 394 nm) corresponding to the resonant excitation of Eu^{3+} ions and in the charge transfer band maximum (λ_{ex} ~ 260–245 nm). The luminescence spectra of the $Lu_{1-x}Eu_xBO_3$ samples at $0 \le x \le 0.07$ having, according to the X-ray analysis data, the calcite structure (Table 1) are identical. In these samples, the luminescence spectra of the near-surface layer (λ_{ex} = 260 nm) and the sample bulk (λ_{ex} = 394 nm) coincide (Fig. 7, spectra *1* and *2*). They contain the bands with λ_{max} = 589.8 and 595.7 nm characteristic of the calcite modification $LuBO_3$ (Eu) [2, 22, 23]. In the $Lu_{0.91}Eu_{0.09}BO_3$ samples, the luminescence spectrum of the near-surface layer (λ_{ex} = 250 nm) contains the bands with λ_{max} = 589.8 and 595.7 nm characteristic of the calcite modification $Lu_{1-x}Eu_xBO_3$ (Fig. 7, spectrum *3*). At the same time, the luminescence spectrum of the sample bulk (λ_{ex} = 394 nm) contains as the bands characteristic of the calcite modification, so the bands corresponding to the vaterite structure of these microcrystals (Fig. 7, spectrum *4*). In the $Lu_{0.91}Eu_{0.09}BO_3$ samples containing 13.5% vaterite (Table 1), the amount of fine 1–2-μm microcrystals having the vaterite structure is only ~0.4% (Subsection 4.1, Fig. 3b). Thus, a significant fraction of the vaterite $Lu_{0.91}Eu_{0.09}BO_3$ phase is contained in the 15–20-μm microcrystals. The appearance of the bands of 588–596, 608–613, and 624–632 nm in the luminescence spectrum during the resonant excitation of Eu^{3+} ions (λ_{ex} = 394 nm) demonstrates that the vaterite modification in these samples forms in the bulk of coarse 15–20-μm microcrystals, while their near-surface layer has still the calcite structure. Further increase in the europium concentration leads to the appearance of the vaterite phase also in the near-surface layer of the microcrystals. In the $Lu_{0.885}Eu_{0.115}BO_3$ samples, the luminescence spectra of the sample bulk and near-surface layer contain the bands characteristic of the calcite (589.8 and 595.7 nm) and vaterite (588–596, 608–613, and 624–632 nm) phases (Fig. 7, spectra *5* and *6*). These samples contain 36% calcite and 64% vaterite. The luminescence spectra of the near-surface layer and the bulk of the $Lu_{0.8}Eu_{0.2}BO_3$ sample contain only the bands characteristic of the vaterite modification of $LuBO_3$ (Eu) (Fig. 7, spectra *7* and *8*). These samples consist of the majority of the 1–2-μm microcrystals. This fact shows that the 1–2-μm microcrystals of orthoborates $Lu_{1-x}Eu_xBO_3$ have the vaterite structure, as well as the 1–2-μm $Lu_{0.99-x}Gd_xEu_{0.01}BO_3$ microcrystals [18].

It is important to note that the conclusion that the vaterite phase forms in the bulk of the microcrystals having the calcite structure is confirmed by the results of studying orthoborates $*Lu_{0.85}Eu_{0.15}BO_3$ subjected to pressing before annealing. The mean size of the microcrystals of these samples is 8–15 μm, and the number of fine 1–2-μm microcrystals is very small (Fig. 3e). In the luminescence spectrum of these samples bulk containing 25% calcite phase and 75% vaterite phase (Table 1) (Fig. 7, spectrum *10*), there are only the bands characteristic of the vaterite $LuBO_3$ (Eu) phase. At the same time, the luminescence spectrum of the near-surface layer contains the bands of the calcite and vaterite modifications of $LuBO_3$ (Eu) (Fig. 7, spectrum *9*).

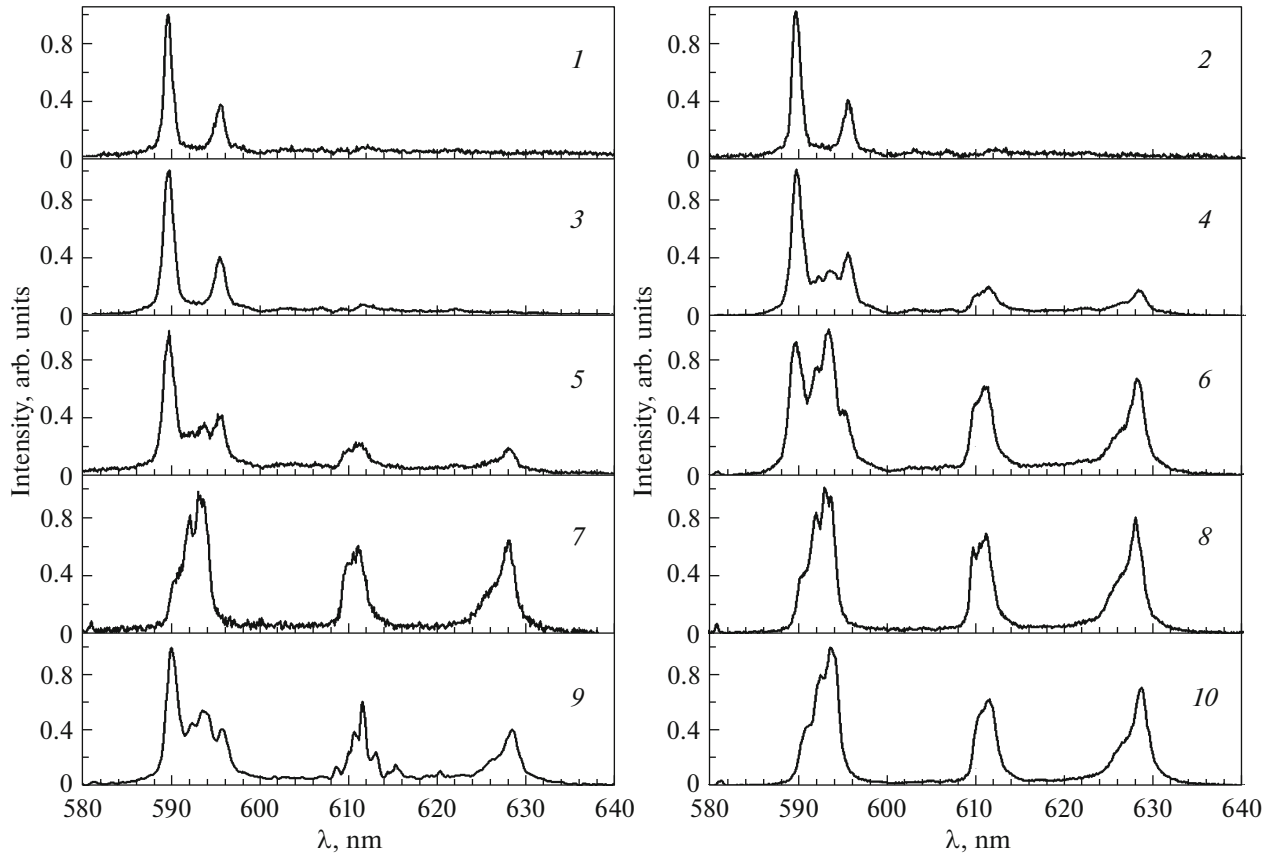

Fig. 7. Luminescence spectra of orthoborates $Lu_{1-x}Eu_xBO_3$: (*1*, *2*) $Lu_{0.93}Eu_{0.07}BO_3$, (*3*, *4*) $Lu_{0.91}Eu_{0.09}BO_3$, (*5*, *6*) $Lu_{0.885}Eu_{0.115}BO_3$, (*7*, *8*) $Lu_{0.8}Eu_{0.2}BO_3$, (*9*, *10*) *$Lu_{0.85}Eu_{0.15}BO_3$; (*1*) $\lambda_{ex} = 260$ nm; (*3*, *9*) $\lambda_{ex} = 250$ nm; (*5*, *7*) $\lambda_{ex} = 245$ nm; (*2*, *4*, *6*, *8*, *10*) $\lambda_{ex} = 394$. *$Lu_{0.85}Eu_{0.15}BO_3$ is the sample subjected to pressing before annealing.

Figure 8 shows the luminescence spectra of orthoborates $Lu_{0.99-x}Tb_xEu_{0.01}BO_3$. In these compounds, the changes in the luminescence spectra due to an increase in the Tb^{3+} concentration are similar to the changes observed in orthoborates $Lu_{1-x}Eu_xBO_3$. At $0 \le x < 0.09$, the $Lu_{0.99-x}Tb_xEu_{0.01}BO_3$ samples are single-phase and have the calcite structure (Table 1). The luminescence spectra of these samples coincide. Figure 8 (spectra *1* and *2*) show, as an example, the luminescence spectra of the near-surface layer (λ_{ex} = 250 nm) and the bulk (λ_{ex} = 378 nm) of the $Lu_{0.92}Tb_{0.07}Eu_{0.01}BO_3$ samples. They contain bands at 589.8 and 595.7 nm characteristic of calcite modification of $LuBO_3$ (Eu). The luminescence spectrum of the near-surface layer (λ_{ex} = 250 nm) of the $Lu_{0.885}Tb_{0.105}Eu_{0.01}BO_3$ samples also contains the bands corresponding to the calcite modification of $LuBO_3$ (Eu) (Fig. 8, spectrum *3*). At the same time, when exciting the bulks of these samples (λ_{ex} = 378 nm), we observe as the bands characteristic of the calcite and the vaterite structures of these samples (Fig. 8, spectrum *4*). In the $Lu_{0.885}Tb_{0.105}Eu_{0.01}BO_3$ samples containing 21% vaterite (Table 1), the summary volume of the fine 1–2-μm with the vaterite structure is only ~2% (Subsection 4.1, Fig. 3g). Thus, the main fraction of the vaterite $Lu_{0.91}Eu_{0.09}BO_3$ phase is contained in the 15–20 μm microcrystals. The appearance of the bands of 588–596 nm, 608–613 nm, and 624–632 nm in the luminescence spectrum of the bulk of these microcrystals (λ_{ex} = 378 nm) demonstrates that the vaterite modification in coarse 15–20 μm microcrystals of the $Lu_{0.99-x}Tb_xEu_{0.01}BO_3$ samples forms in their bulks. With a further increase in the concentration of Tb^{3+} the vaterite phase is also formed in the near-surface layer microcrystals. In the orthoborates $Lu_{0.84}Tb_{0.15}Eu_{0.01}BO_3$ containing 86% vaterite, the luminescence spectrum of the sample bulk contains only the bands characteristic of the vaterite modification, while the spectrum of the near-surface layer has the bands characteristic of the calcite and also the vaterite structures of these samples (Fig. 8, spectra *5* and *6*). At the concentration 20 at % Tb^{3+} ions, the luminescence spectra of the bulk and the near-resistance layer have the bands characteristic of only the vaterite modification of $Lu_{0.99-x}Tb_xEu_{0.01}BO_3$ (Fig. 8, spectra *7* and *8*).

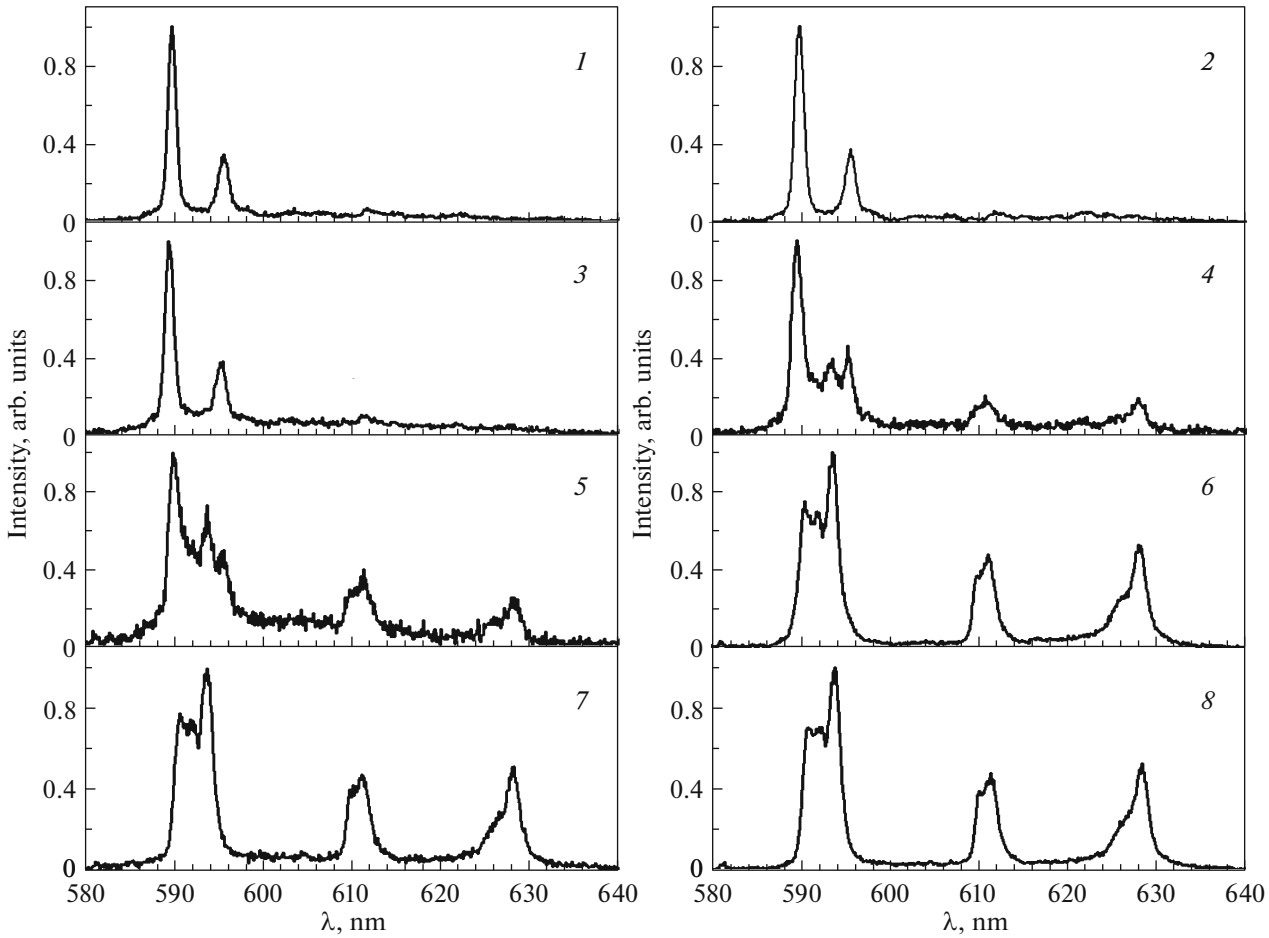

Fig. 8. Luminescence spectra of orthoborates $Lu_{0.99-x}Tb_xEu_{0.01}BO_3$: (*1*, *2*) $Lu_{0.92}Tb_{0.07}Eu_{0.01}BO_3$; (*3*, *4*) $Lu_{0.885}Tb_{0.105}Eu_{0.01}BO_3$; (*5*, *6*) $Lu_{0.84}Tb_{0.15}Eu_{0.01}BO_3$; (*7*, *8*) $Lu_{0.79}Tb_{0.2}Eu_{0.01}BO_3$; (*1*, *3*, and *5*) λ_{ex} = 250 nm; (*7*) λ_{ex} = 245 nm; (*2*, *4*, *6*, and *8*) λ_{ex} = 378 nm.

6.3. Luminescence Spectra of the $Lu_{0.99-x}Y_xEu_{0.01}BO_3$ Orthoborates

As noted in Subsection 4.2, the morphology of the $Lu_{0.99-x}Y_xEu_{0.01}BO_3$ orthoborates noticeably differs from the morphologies of the $Lu_{1-x}Eu_xBO_3$ and $Lu_{0.99-x}Tb_xEu_{0.01}BO_3$ compounds. The $Lu_{0.99-x}Y_xEu_{0.01}BO_3$ samples in the Y^{3+} concentration range under study consist mainly of 8–20 μm microcrystals, and the content of the fine 1–2 μm microcrystals is very low. The highest content of the fine 1–2-μm microcrystals (~1% of the whole volume) is observed in the $Lu_{0.84}Y_{0.15}Eu_{0.01}BO_3$ (Fig. 4b); at the same time, this sample contains 20% vaterite phase (Table 1), which shows that the main fraction of the vaterite phase is contained in the 8–20 μm microcrystals. It should be noted, as well, that the pressing of the tablets before annealing at 970°C only slightly influences the morphology of $Lu_{0.99-x}Y_xEu_{0.01}BO_3$; in these samples, at $0.1 < x \le 0.25$, there are 8–20 μm microcrystals.

Figure 9 (spectra *1*–*8*) shows the luminescence spectra (LS) of the $Lu_{0.99-x}Y_xEu_{0.01}BO_3$ compounds containing 10, 15, 20, and 25 at % Y^{3+} excited by the light corresponding to the resonant excitation of Eu^{3+} ions (λ_{ex} = 394 nm) and in the maximum of the charge transfer band (λ_{ex} ~ 250–243 nm). LS of these samples, which have the calcite structure at $0 \le x < 0.1$ (Table 1), according to the X-ray phase analysis data, are identical. In these samples, the luminescence spectra of the near-surface layer (λ_{ex} = 250 nm) and the sample bulk (λ_{ex} = 394 nm) coincide (Fig. 9, spectra *1* and *2*). They contain the bands with λ_{max} = 589.8 and 595.7 nm characteristic of the calcite modification of $LuBO_3$ (Eu). In the $Lu_{0.84}Y_{0.15}Eu_{0.01}BO_3$ samples containing 80% calcite and 20% vaterite (Table 1), LS of the near-surface layer contains only the bands characteristic of the calcite modification of $LuBO_3$(Eu) (Fig. 9, spectrum *3*). At the same time, in LS of the bulk of these microcrystals, there are bands characteristic both the calcite and vaterite modifications (588–596, 608–613, and 624–632 nm) of these compounds

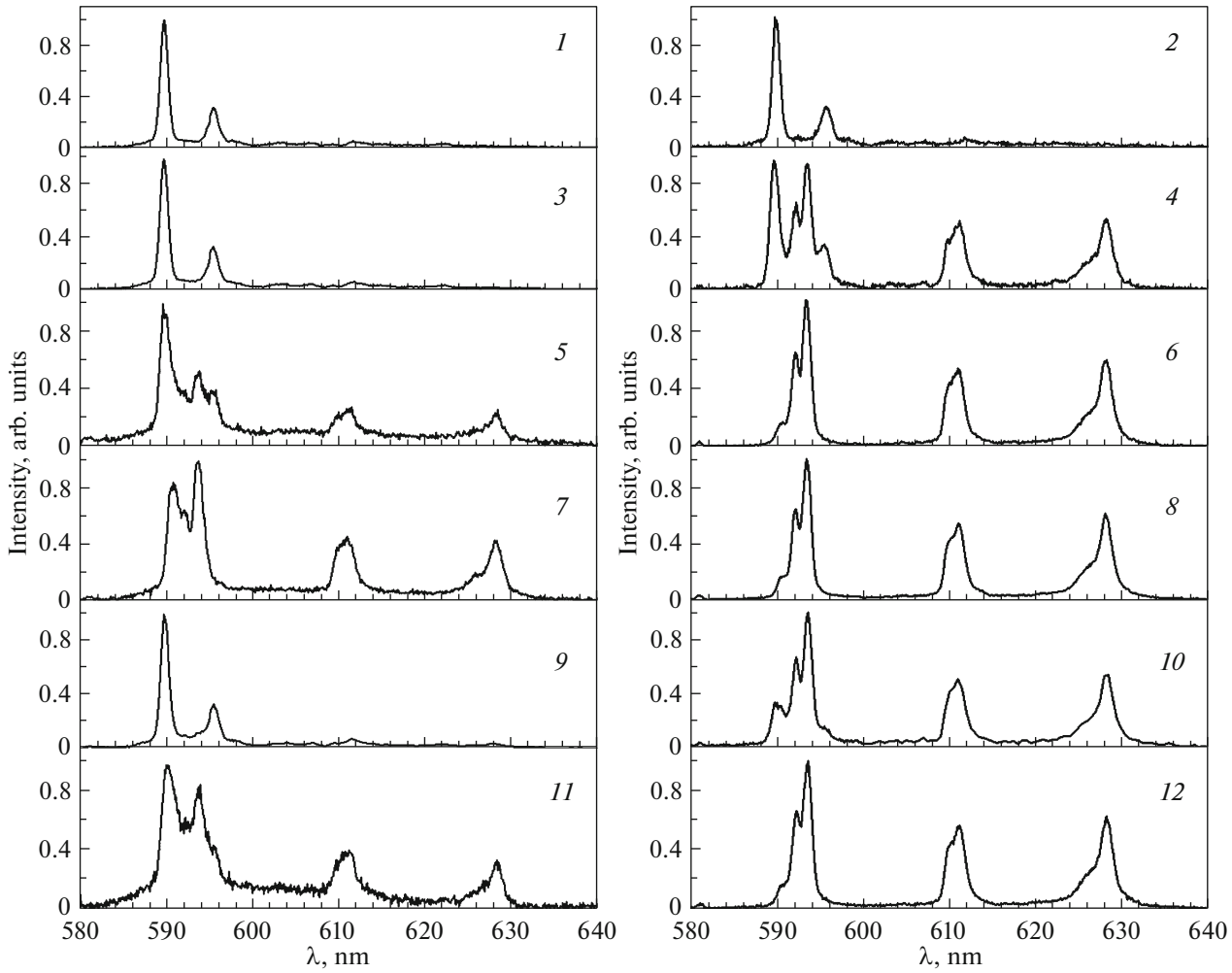

Fig. 9. Luminescence spectra of orthoborates $Lu_{0.99-x}Y_xEu_{0.01}BO_3$: (*1*, *2*) $Lu_{0.89}Y_{0.1}Eu_{0.01}BO_3$; (*3*, *4*) $Lu_{0.84}Y_{0.15}Eu_{0.01}BO_3$; (*5*, *6*) $Lu_{0.79}Y_{0.2}Eu_{0.01}BO_3$; (*7*, *8*) $Lu_{0.74}Y_{0.25}Eu_{0.01}BO_3$; (*9*, *10*) $*Lu_{0.84}Y_{0.15}Eu_{0.01}BO_3$; (*11*, *12*) $*Lu_{0.79}Y_{0.2}Eu_{0.01}BO_3$ ((*1*, *3*, and *9*) λ_{ex} = 250 nm; (*5*, *7*, and *11*) λ_{ex} = 243 nm; (*2*, *4*, *6*, *8*, *10*, and *12*) λ_{ex} = 394 nm). $*Lu_{0.84}Y_{0.15}Eu_{0.01}BO_3$ and $*Lu_{0.79}Y_{0.2}Eu_{0.01}BO_3$ are the samples subjected to pressing before annealing.

(Fig. 9, spectrum *4*). These results demonstrate that the vaterite phase form first in the coarse 8–20-μm microcrystals.

The luminescence spectra of the bulks of the $Lu_{0.79}Y_{0.2}Eu_{0.01}BO_3$ samples containing 10% calcite and 90% vaterite contain only the bands characteristic of the vaterite modification of $LuBO_3$ (Eu) (Fig. 9, spectrum *6*). At the same time, LS of the near-surface layer contains as the bands characteristic of the calcite modification (589.8 and 595.7 nm), so the bands characteristic of the vaterite modification of these compounds (Fig. 9, spectrum *5*). LS of the near-surface and the bulk of the $Lu_{0.74}Y_{0.25}Eu_{0.01}BO_3$ orthoborate, which has the vaterite structure (Table 1), contains only the bands observed in the vaterite modification of these samples (Fig. 9, spectra *7* and *8*).

Figure 9 (spectra *9*–*12*) shows the luminescence spectra (LS) of the $Lu_{0.99-x}Y_xEu_{0.01}BO_3$ samples, which were preliminarily subjected to pressing before the annealing. In the luminescence spectrum of the near-surface layer of the $*Lu_{0.84}Y_{0.15}Eu_{0.01}BO_3$ samples containing 52% calcite and 48% vaterite contain only the bands of the calcite modification of $LuBO_3$ (Eu) (589.8 and 595.7 nm) (Fig. 9, spectrum *9*). In the luminescence spectra of the bulk of the $*Lu_{0.84}Y_{0.15}Eu_{0.01}BO_3$ microcrystals, the highest intensity is observed for the bands characteristic of the vaterite modification of these sample, whereas these spectra contain weak bands of the calcite modification of these orthoborates (Fig. 9, spectrum *10*). The luminescence spectra of the bulks and the near-surface layer of the $*Lu_{0.79}Y_{0.2}Eu_{0.01}BO_3$ microcrystals contain only the bands characteristic of the vaterite structure of these compounds (Fig. 9, spectra *11* and *12*). According to the X-ray phase analysis data, these sam-

ples contain 4.5% calcite phase and 95.5% vaterite phase (Table 1).

Thus, based on the studies of the luminescence spectra of the near-surface layer and the bulk of the $Lu_{0.99-x}Y_xEu_{0.01}BO_3$ orthoborates, it can be concluded that, at the Y^{3+} concentrations $x > 0.1$, the vaterite phase forms first in the bulk of the coarse 8–20 μm microcrystals.

It is important to note that the study of the luminescence spectra at various wavelength of the exciting light enables one to observe the process of formation of structural modifications in the bulk and on the surface of microcrystals of the samples studied in this work as the doping impurity concentration increases.

It is shown that the luminescence spectra of the near-surface layer and the bulk of the $Lu_{1-x}RE_xBO_3$ (RE = Eu, Tb, and Y) microcrystals, having in all the volume the calcite or vaterite structures, coincide and contain the luminescence bands characteristic of these phases: 589.8 and 595.7 nm for the calcite phase, and 588–596, 608–613, and 624–632 nm, for vaterite.

It is found that the vaterite phase in the two-phase range forms, first, in the bulk of the coarse 8–20-μm particles which had the calcite structure. As the RE ion concentration increases, the vaterite phase also forms on the surface of these microcrystal.

In $LuBO_3$ borates, the vaterite phase density (7.42 g/cc) is markedly higher than the calcite phase density (6.871 g/cc) [20]; thus, as the vaterite phase forms in the bulk of coarse microcrystals with the calcite structure, the mechanical stresses retarding to this process will not appear. Since the vaterite phase has a smaller volume, the formation of the vaterite phase in the calcite microcrystals, voids form in them; the void aggregation can lead to a continuity violation and the crack formation which are observed experimentally (Figs. 3e, 3m, and 3n; Figs. 4c, 4d, 4e, 4f, 4g, and 4h).

It should be noted that the X-ray phase analysis gives the information on the sample structure averaged over its volume, since the penetration depth of the X-ray radiation and the maximum size of the microcrystals under study are close to one another and are ~10–15 μm. At the same time, as noted above, the structures on the surface and in the bulk of a sample can be substantially different [14–16]. Thus, the use of optically active and structurally-sensitive marks makes it possible to study the structure of the near-surface layer and the bulk of the $Lu_{1-x}RE_xBO_3$ sample in the dependence on the RE^{3+} concentration and to obtain more complete information on the changes in the structural states of the compounds under study.

7. CONCLUSIONS

In this work, the structure, the morphology, the IR absorption spectra, the luminescence excitation spectra, and the luminescence spectra of the near-surface layer and the bulk of microcrystals of orthoborates $Lu_{1-x}Eu_xBO_3$, $Lu_{0.99-x}Tb_xEu_{0.01}BO_3$ with $0 \le x \le 0.20$ and $Lu_{0.99-x}Y_xEu_{0.01}BO_3$ with $0 \le x \le 0.25$ synthesized at 970°C have been studied.

It is found that there is the unambiguous correspondence between the structural modification and the spectral characteristics of the photoluminescence and the IR absorption of orthoborates $Lu_{1-x}RE_xBO_3$ (RE = Eu, Tb, and Y).

The study of the luminescence spectra at various wavelengths of the exciting light allowed us to obtain information on the structure of the near-surface layer and the bulk of the samples under study.

It is shown that an increase in the RE concentration in ortoborates $Lu_{1-x}RE_xBO_3$ (RE = Eu, Tb, and Y) leads to a sequential change in the structural state and spectral characteristics.

– $Lu_{1-x}Eu_xBO_3$ at $0 \le x \le 0.07$,

$Lu_{0.99-x}Tb_xEu_{0.01}BO_3$ at $0 \le x \le 0.09$

and $Lu_{0.99-x}Y_xEu_{0.01}BO_3$ at $0 \le x \le 0.1$

are single-phase and have the calcite structure (space group $R\bar{3}c$). The luminescence spectra of the Eu^{3+} ions in the near-surface layer and in the bulk of the microcrystals of these samples, corresponding to this structure, contain the bands characteristic of the calcite modification (λ_{max} = 589.8 and 595.7 nm).

– $Lu_{1-x}Eu_xBO_3$, $Lu_{0.99-x}Tb_xEu_{0.01}BO_3$ at $x \ge 0.2$

and $Lu_{0.99-x}Y_xEu_{0.01}BO_3$ at $x \ge 0.25$

have the vaterite structure (space group $C2/c$) over entire volume. The luminescence spectra of the Eu^{3+} ions in the near-surface layer and the bulk of microcrystals in these samples contain the bands characteristic of the vaterite modifications: 588–596, 608–613, and 624–632 nm.

– $Lu_{1-x}Eu_xBO_3$ at $0.07 < x < 0.2$,

$Lu_{0.99-x}Tb_xEu_{0.01}BO_3$ at $0.09 < x < 0.2$

and $Lu_{0.99-x}Y_xEu_{0.01}BO_3$ at $0.1 < x < 0.25$

are two-phase. They contain the calcite and vaterite phases. In the luminescence spectra, there are bands characteristic of the calcite and vaterite modifications of these samples.

The orthoborates $Lu_{0.99-x}Y_xEu_{0.01}BO_3$ having the vaterite structure mainly consist of the 8–20 μm microcrystals, while the $Lu_{1-x}Eu_xBO_3$ and $Lu_{0.99-x}Tb_xEu_{0.01}BO_3$ samples with the vaterite structure consist of the 1–2-μm microcrystals.

It is found that, in the two-phase region, the vaterite phase forms as the 1–2-μm microcrystals, and also in the bulk of the coarse 8–20-μm microcrystals, as is the case in the $Lu_{0.99-x}Gd_xEu_{0.01}BO_3$.

The orthoborates $Lu_{1-x}Eu_xBO_3$, $Lu_{0.99-x}Tb_xEu_{0.01}BO_3$, and $Lu_{0.99-x}Y_xEu_{0.01}BO_3$ have the high luminescence intensity and can be used as efficient red luminophors for LED light sources.

ACKNOWLEDGMENTS

The authors are grateful to the research facility unit of the Osipyan Institute of Solid State Physics of the Russian Academy of Sciences for the morphology study of the samples, as well as their characterization by IR spectroscopy and X-ray diffraction analysis.

FUNDING

The research is carried out within the state task of ISSP RAS.

CONFLICT OF INTEREST

The authors declare that they have no conflicts of interest.

REFERENCES

1. Y. H. Zhou, J. Lin, S. B. Wang, and H. J. Zhang, Opt. Mater. **20**, 13 (2002).
2. Jun Yang, Chunxia Li, Xiaoming Zhang, Zewei Quan, Cuimiao Zhang, Huaiyong Li, and Jun Lin, Chem. Eur. J. **14**, 4336 (2008).
3. C. Mansuy, J. M. Nedelec, C. Dujardin, and R. Mahiou, Opt. Mater. **29**, 697 (2007).
4. J. Yang, G. Zhang, L. Wang, Z. You, S. Huang, H. Lian, and J. Lin, J. Solid State Chem. **181**, 2672 (2008).
5. S. Z. Shmurak, A. P. Kiselev, V. V. Sinitsyn, I. M. Shmyt'ko, A. S. Aronin, B. S. Red'kin, and E. G. Ponyatovskii, Phys. Solid State **48**, 51 (2006).
6. S. Z. Shmurak, V. V. Kedrov, A. P. Kiselev, and I. I. Zver'kova, Phys. Solid State **55**, 377 (2013).
7. A. A. Mazilkin, O. G. Rybchenko, T. N. Fursova, S. Z. Shmurak, and V. V. Kedrov, Mater. Charact. **147**, 215 (2019).
8. S. Z. Shmurak, V. V. Kedrov, A. P. Kiselev, T. N. Fursova, and I. M. Shmyt'ko, Phys. Solid State **58**, 578 (2016).
9. S. Z. Shmurak, V. V. Kedrov, A. P. Kiselev, T. N. Fursova, and O. G. Rybchenko, Phys. Solid State **59**, 1171 (2017).
10. S. Z. Shmurak, V. V. Kedrov, A. P. Kiselev, T. N. Fursova, I. I. Zver'kova, and S. S. Khasanov, Phys. Solid State **62**, 2122 (2020).
11. S. Z. Shmurak, V. V. Kedrov, A. P. Kiselev, T. N. Fursova, I. I. Zver'kova, and S. S. Khasanov, Phys. Solid State **62**, 2374 (2020).
12. M. A. El'yashevich, *Spectroscopy of Rare Earths* (GITTL, Moscow, 1953) [in Russian].
13. M. I. Gaiduk, V. F. Zolin, and L. S. Gaigerova, *Luminescence Spectra of Europium* (Nauka, Moscow, 1974) [in Russian].
14. A. P. Kiselev, S. Z. Shmurak, B. S. Red'kin, V. V. Sinitsyn, I. M. Shmyt'ko, E. A. Kudrenko, and E. G. Ponyatovskii, Phys. Solid State **48**, 1544 (2006).
15. S. Z. Shmurak, A. P. Kiselev, N. V. Klassen, V. V. Sinitsyn, I. M. Shmyt'ko, B. S. Red'kin, and S. S. Khasanov, IEEE Trans. Nucl. Sci. **55**, 1128 (2008).
16. S. Z. Shmurak, A. P. Kiselev, D. M. Kurmasheva, B. S. Red'kin, and V. V. Sinitsyn, J. Exp. Theor. Phys. **110**, 759 (2010).
17. D. Hrrniak, E. Zych, L. Kepinski, and W. Strek, J. Phys. Chem. Solids **64**, 11 (2003).
18. S. Z. Shmurak, V. V. Kedrov, A. P. Kiselev, T. N. Fursova, I. I. Zver'kova, and E. Yu. Postnova, Phys. Solid State **63** (2021, in press).
19. J. Hölsä, Inorg. Chim. Acta **139**, 257 (1987).
20. E. M. Levin, R. S. Roth, and J. B. Martin, Am. Miner. **46**, 1030 (1961).
21. G. Chadeyron, M. El-Ghozzi, R. Mahiou, A. Arbus, and C. Cousseins, J. Solid State Chem. **128**, 261 (1997).
22. S. Z. Shmurak, V. V. Kedrov, A. P. Kiselev, and I. M. Shmyt'ko, Phys. Solid State **57**, 18 (2015).
23. S. Z. Shmurak, V. V. Kedrov, A. P. Kiselev, T. N. Fursova, and I. M. Shmyt'ko, Phys. Solid State **57**, 1588 (2015).
24. D. Santamaría-Pérez, O. Gomis, J. Angel Sans, H. M. Ortiz, A. Vegas, D. Errandonea, J. Ruiz-Fuertes, D. Martinez-Garcia, B. Garcia-Domene, L. André, J. Pereira, F. Javier Manjón, P. Rodríguez-Hernández, A. Muñoz, F. Piccinelli, M. Bettinelli, and C. Popescu, J. Phys. Chem. C **118**, 4354 (2014).
25. W. Ding, P. Liang, and Zh.-H. Liu, Mater. Res. Bull. **94**, 31 (2017).
26. W. Ding, P. Liang, and Zh.-H. Liu, Solid State Sci. **67**, 76 (2017).
27. Zh.-J. Zhang, T.-T. Jin, M.-M. Xu, Q.-Zh. Huang, M.-R. Li, and J.-T. Zhao, Inorg. Chem. **54**, 969 (2015).
28. A. G. Ryabukhin, Izv. Chelyab. Nauch. Tsentra, No. 4, 33 (2000).
29. S. Z. Shmurak, V. V. Kedrov, A. P. Kiselev, T. N. Fursova, I. I. Zver'kova, and S. S. Khasanov, Phys. Solid State **61**, 632 (2019).
30. S. Z. Shmurak, V. V. Kedrov, A. P. Kiselev, T. N. Fursova, I. I. Zver'kova, and S. S. Khasanov, Phys. Solid State **61**, 2117 (2019).
31. C. E. Weir and E. R. Lippincott, J. Res. Natl. Bur. Stand. A **65**, 173 (1961).
32. D. Boyer, F. Leroux, G. Bertrand, and R. Mahiou, J. Non-Cryst. Solids **306**, 110 (2002).
33. J. P. Laperches and P. Tarte, Spectrochim. Acta **22**, 1201 (1966).
34. A. Szczeszak, T. Grzyb, S. Lis, and R. J. Wiglusz, Dalton Trans. **41**, 5824 (2012).
35. G. Jia, P. A. Tanner, Ch.-K. Duan, and J. Dexpert-Ghys, J. Phys. Chem. C **114**, 2769 (2010).

Translated by Yu. Ryzhkov